

## MEMS-FABRICATED GYROSCOPES WITH FEEDBACK COMPENSATION

**Yonghwa Park\*, Sangjun Park\*, Byung-doo Choi\*, Hyoungho Ko\*, Taeyong Song\*, Geunwon Lim\*, Kwangho Yoo\*\*\*, Sangmin Lee\*, Sang Chul Lee\*\*\*, Ahra Lee\*\*\*, Jaesang Lim\*\*, Seongssoo Hong\*, Kunsoo Huh\*\*\*, Jahng-hyon Park\*\*\*, and Dong-il "Dan" Cho\*\*\*,+<sup>†</sup>**

\*School of Electrical Engineering and Computer Science, Seoul National University,  
San 56-1, Shinlim-dong, Kwanak-gu, Seoul 151-742, Korea

\*\*SML Electronics, Inc., Seoul, Korea

\*\*\*School of Mechanical Engineering, Hanyang University, Seoul, Korea

**Abstract:** This paper presents a lead-lag compensator design for a MEMS-fabricated microgyroscope. The microgyroscope is basically a high Q system, thus the bandwidth is limited to be narrow. To overcome the open-loop performance limitations, a feedback controller is designed to improve the resolution, bandwidth, linearity, and bias stability of the microgyroscope. The feedback controller is applied to the z-axis microgyroscope fabricated by SBM process. In MATLAB simulations, resolution, bandwidth, input range, and bias stability of closed-loop system are improved from 0.0021 deg/sec to 0.0013 deg/sec, from 14.8 Hz to 115 Hz, from  $\pm 50$  deg/sec to  $\pm 200$  deg/sec, and from 0.0249 deg/sec to 0.0028 deg/sec, respectively. Copyright © 2005 IFAC

**Keywords:** Gyroscopes, Performance limits, Feedback control, Modelling, Simulation

### 1. INTRODUCTION

Micro-fabricated gyroscopes have received much commercial attraction due to the small size, low power consumption, rigidity, and low cost. Application areas of the microgyroscope include automotive safety and stability control systems, video camera stabilization, and 3-D input devices for computers and personal data assistance (PDA) systems (Song, 1977; Gripton, 2002).

The feedback controller is applied to the z-axis microgyroscope fabricated by the Sacrificial Bulk Micromachining (SBM) process. The performances of this open-loop gyroscope are represented in the literature (Lee, et al., 2000; Cho, et al., 2000; Park, et al., 2001). The non-linear output characteristic and small bandwidth are main problems of this microgyroscope.

Because the resonant frequencies of the decoupled microgyroscope should be matched identically and the system has a very high Q, the gyroscope operates at a narrow bandwidth near a specific resonant frequency. In the open-loop system, if the bandwidth of the system can be increased by increasing the

difference of two resonant modes, but then the sensitivity of this system becomes poor. To ameliorate this trade-off problem, we design a feedback controller in this paper. The closed-loop system feeds the control signal from the sensed output signal back to the feedback control electrodes. This makes a displacement of the moving parts very small, and the bandwidth of the system is increased without lowering the sensitivity. Furthermore, because the displacement of the moving parts is controlled to be small, the linearity of the output signal can be improved.

### 2. WORKING PRINCIPLE

Figure 1 shows the z-axis microgyroscope fabricated by sacrificial bulk micromachining (SBM) process. The structural thickness is 40  $\mu\text{m}$ , and the sacrificial gap is 20  $\mu\text{m}$ . The SBM process has the added benefits of a large sacrificial gap when compared to conventional SOI process (Lee, et al., 1999; Lee, et al., 2000; Cho, et al., 2000).

<sup>†</sup> Corresponding author, Phone: +82.2.880.8371, Fax: +82.2.877.9304, E-mail: [dicho@asri.snu.ac.kr](mailto:dicho@asri.snu.ac.kr)

The schematic of the fabricated microgyroscope can be represented as shown in Figure 2. The outer and inner masses are driven together in the x-direction at the driving mode. If an angular rate is applied in the z-direction, then the inner mass moves in the y-direction by the Coriolis force. That is, the microgyroscope estimates the input angular rate by sensing the displacement of the inner mass induced by the Coriolis force.

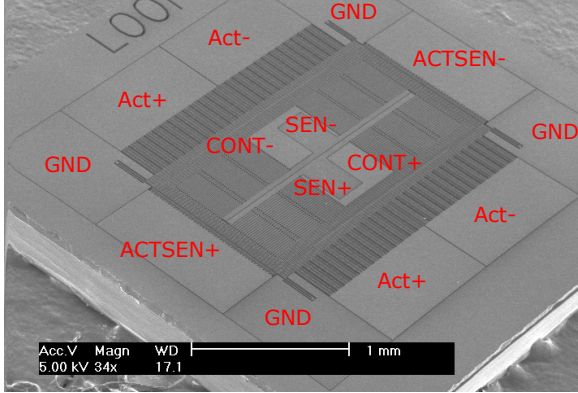


Fig. 1. Fabricated microgyroscope

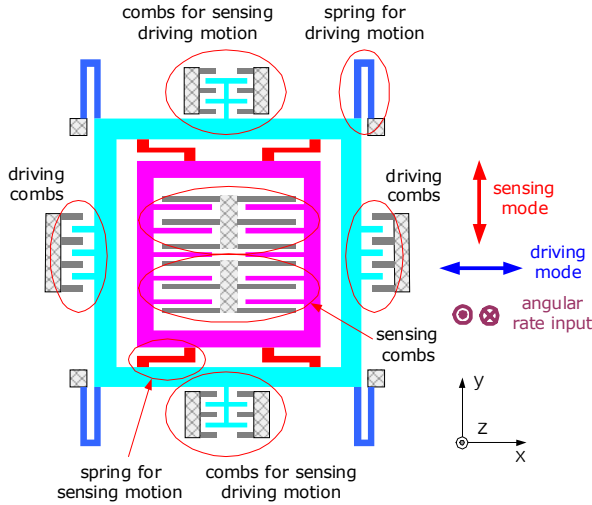


Fig. 2. Schematic diagram of microgyroscope.

### 3. DYNAMIC MODELLING

#### 3.1 Microgyroscope

The dynamics of the microgyroscope can be modelled as two orthogonal mass-damper-spring systems as shown in Figure 3. The motion equations of plant dynamics are given by

$$\text{Driving part: } (m_a + m_s)\ddot{x} + b_a\dot{x} + k_a x = F_e \quad (1)$$

$$\text{Sensing part: } m_s\ddot{y} + b_s\dot{y} + k_s y = F_c = 2m_s\Omega_z v_x \quad (2)$$

where  $m_a$ ,  $b_a$ ,  $k_a$  are mass, damping and spring coefficient of the driving part, respectively;  $m_s$ ,  $b_s$ ,  $k_s$  are mass, damping and spring coefficient of the sensing part, respectively;  $F_e$  is driving force,  $F_c$  is coriolis force,  $v_x$  is velocity of the mass which

oscillates in sinusoidal motion by driving force, and  $\Omega_z$  is input angular rate.

To vibrate the gyroscope in driving mode, a sinusoidal voltage is applied to the driving-comb electrodes. This driving voltage generates the electrostatic force. The driving force is given by

$$F_e = \frac{2N_1\epsilon t V_{off}}{d_d} V_a \quad (3)$$

where  $N_1$ ,  $\epsilon$ ,  $d_d$ ,  $t$ ,  $V_{off}$ , and  $V_a$  are number of driving combs, permittivity, gap between driving combs, structural thickness, offset voltage of carrier signal and ac voltage of carrier signal, respectively. The value of calculated  $F_e$  is  $4.6 \times 10^{-7} V_a N$ .

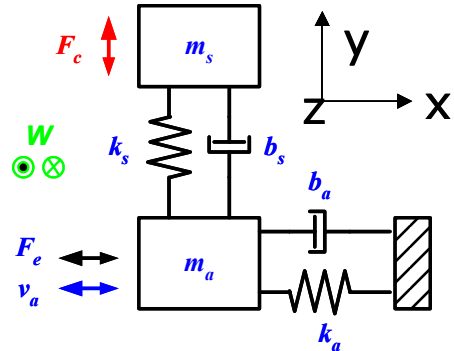


Fig. 3. Modeling of microgyroscope.

The values of  $m$ ,  $b$ , and  $k$  can be obtained from the structure of the microgyroscope and the equations of relation between the resonant frequency, quality factor, and damping coefficient. The resonant frequency and quality factor are given by

$$f = \frac{1}{2\pi} \sqrt{\frac{k}{m}} \quad (4)$$

$$\frac{1}{Q} = \frac{\mu A \beta}{\sqrt{mk} \left( \frac{\cosh 2\beta d - \cos 2\beta d}{\sinh 2\beta d + \sin 2\beta d} \right)} + \frac{\mu A_c \beta}{\sqrt{mk} \left( \frac{\cosh 2\beta d_c - \cos 2\beta d_c}{\sinh 2\beta d_c + \sin 2\beta d_c} \right)} + \frac{\mu t W^3}{d_2^3 \sqrt{mk}} \quad (5)$$

where  $\mu$ ,  $\beta$ ,  $A$ ,  $A_c$ ,  $d$ ,  $d_c$ ,  $d_2$ , and  $W$  are absolute viscosity, momentum propagation velocity, area of plate, areas of inter-comb, sacrificial gap, lateral gap between combs, gap between structure and comb, and width of comb, respectively (Cho, et al., 1993). Because the fabricated microgyroscope is tested in vacuum environment, the vacuum level is also important. The damping coefficient is given by

$$b = \frac{\sqrt{mk}}{Q}. \quad (6)$$

The calculated mass,  $m_a$  and  $m_s$ , are  $78.3 \mu\text{g}$  and  $42.6 \mu\text{g}$ , respectively. By ANSYS simulation, the first mode resonant frequency of the driving mode is 5.04

kHz. The resonant frequencies of the driving and sensing modes should be matched to achieve a sensitivity of the system. The sensing mode resonant frequency is tuned to be 10 Hz higher than the driving mode, that is, 5.05 kHz. From Eq. (4), the values of  $k_a$  and  $k_s$  are 121.2 N/m and 42.85 N/m, respectively. From Eqs. (5) - (6) and the vacuum level, the values of  $b_a$  and  $b_s$  are  $3.83 \times 10^{-6}$  kg/s and  $1.35 \times 10^{-6}$  kg/s, respectively. Therefore, from Eqs. (1) - (3), the transfer functions of the driving part and the sensing part become

$$T_d(s) = \frac{X(s)}{V_a(s)} = \frac{3.807}{s^2 + 31.68s + 1.003 \times 10^9} \quad (7)$$

$$T_s(s) = \frac{Y(s)}{F_c(s)} = \frac{2.35 \times 10^7}{s^2 + 31.68s + 1.007 \times 10^9}. \quad (8)$$

The movement of the sensing-combs in the y-direction by the Coriolis force compels the gap of the sensing-combs to vary, and this variation produces the capacitance change. So, C/Y gain, that is, the ratio of the capacitance change to the movement of the sensing-combs is given by

$$C/Y \text{ Gain} = N_2 \varepsilon A_c \left( \frac{1}{(d_s - y)^2} - \frac{1}{(2d_s - y)^2} \right) \quad (9)$$

where  $N_2$  is number of sensing-combs and  $d_s$  is lateral gap between sensing-combs. When the value of  $y$  is very small, Eq. (9) becomes

$$C/Y \text{ Gain} = \frac{3N_2 \varepsilon A_c}{4d_s^2}. \quad (10)$$

The calculated C/Y gain is  $1.908 \times 10^{-7}$  C/m.

### 3.2 Measurement Circuit

Figure 4 shows the measurement scheme in the open-loop. To vibrate the gyroscope in driving mode, a 1 volt peak-to-peak sinusoidal voltage with a 0.5 volt offset is applied to the driving-comb electrodes. When an angular rate is applied in the z-direction, the sensing-comb electrodes move in the y-direction by the Coriolis force. The capacitance changes due to the motion of the sensing-comb electrodes are detected by a charge-to-voltage converter. To pass only modulated high frequency signals, a high-pass filter is used. After the high-pass filtering, the signal is demodulated using an analog multiplier. After the demodulation, the high frequency components of the signal are removed using low-pass filter, and the angular rate signal is obtained

The transfer function of the charge amplifier  $T_C(s)$  is given by

$$T_C(s) = \frac{V_C(s)}{C(s)} = -\frac{1.05 \times 10^9 s}{s + 2 \times 10^4} V_{ref} \quad (11)$$

where  $C(s)$  is capacitance change,  $V_C(s)$  is output voltage of the charge amplifier, and  $V_{ref}$  is reference voltage. The transfer functions of the high-pass filter  $T_H(s)$  is given by

$$T_H(s) = -\frac{s^2}{s^2 + 3.16 \times 10^3 s + 3.96 \times 10^6}. \quad (12)$$

Also, the gain of the differential amplifier is 5.27 V/V.

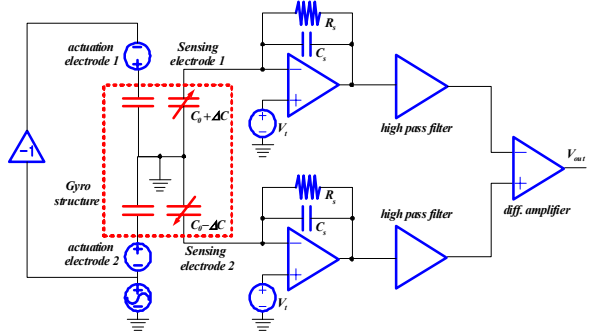


Fig. 4. Measurement scheme of the open-loop.

### 4. CONTROLLER DESIGN

Figure 5 shows the block diagram of the closed-loop system. The closed-loop system feeds the control signal from the modulated output signal back to the feedback control electrodes. The plant  $G(s)$  consists of the sensing dynamics of the microgyroscope, the charge amplifier, the highpass filter, and the differential amplifier as shown in Figure 4. This plant  $G(s)$  is modeled as a 5th-order transfer function. This plant  $G(s)$  is given by

$$G(s) = \frac{6.345 \times 10^{10} s^3}{(s^2 + 32.1s + 1.031 \times 10^9)(s + 2 \times 10^4)} \quad (13)$$

$$\bullet \frac{1}{s^2 + 1.163 \times 10^4 s + 3.955 \times 10^7}$$

If the output voltage of the controller is applied to the feedback control electrodes, the electrostatic force is exerted on the inter-combs. The F/V gain, that is, the ratio of the electrostatic force to the control output voltage is given by

$$F/V \text{ Gain} = \frac{N_2 \varepsilon A_c V_{ref}}{4d_s^2}. \quad (14)$$

The calculated F/V gain is  $1.696 \times 10^{-6}$  N/V.

The 2nd order bandpass filter  $B(s)$  in Figure 5 rejects the noise except the operating frequency. The magnitude and bandwidth of the bandpass filter designed are 0 dB and 1 kHz, and the center frequency of the designed bandpass filter is matched with the resonant frequency of sensing mode, that is, 5.11 kHz. So the bandpass filter  $B(s)$  is given by

$$B(s) = \frac{6283s}{s^2 + 6283s + 1.03 \times 10^9}. \quad (15)$$

The designed lead-lag compensator  $K(s)$  is given by

$$K(S) = \frac{k_l(s + z_{lead})(s + z_{lag})}{(s + p_{lead})(s + p_{lag})} \quad (16)$$

where  $k_l$  is the controller gain;  $z_{lead}$  and  $p_{lead}$  are zero and pole of the lead compensator; and  $z_{lag}$  and  $p_{lag}$  are zero and pole of the lag compensator.

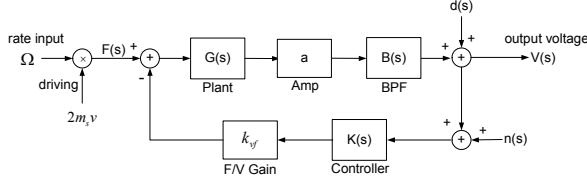


Fig. 5. Block diagram of closed-loop.

The resonant frequencies of the open-loop and closed-loop systems should be matched. From this condition, the below term is given by

$$z_{lead} z_{lag} = \frac{k_s}{m_s}. \quad (17)$$

The magnitudes of the open-loop and closed-loop systems should be also matched at the resonant frequency. From this condition, the below term is given by

$$z_{lead} + z_{lag} = \frac{b_s(a-1)}{ak_{vf}k_{cv}k_l} \quad (18)$$

where  $a$  is proportional coefficient of feedback loop,  $k_{vf}$  is F/V gain, and  $k_{cv}$  is proportional coefficient of charge-to-voltage converter. The value of  $k_{cv}$  is  $5.763 \times 10^4$  V/C.

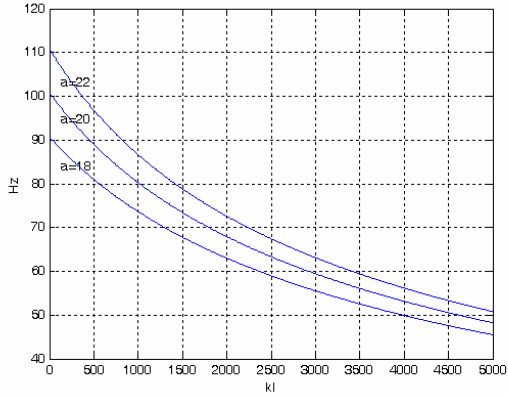


Fig. 6. Bandwidth of closed-loop, when values of  $a$  and  $k_l$  are varied.

First of all, the suitable values of  $p_{lead}$  and  $p_{lag}$  are selected in the neighbourhood of the resonant frequency. When the values of  $p_{lead}$  and  $p_{lag}$  are  $9 \times 10^4$  rad/sec and  $2.5 \times 10^4$  rad/sec, Figure 6 shows the bandwidth of the closed-loop system as the values of  $a$  and  $k_l$  are varied. The bandwidth increases when the value of  $a$  increases, but the noise of system also increases. If the values of  $a$  and  $k_l$  are 22 and 15, then the values of  $z_{lead}$  and  $z_{lag}$  can be obtained from Eqs. (17) and (18). The values of  $z_{lead}$  and  $z_{lag}$  are

$1.36 \times 10^4$  rad/sec and  $7.42 \times 10^4$  rad/sec, and the bandwidth of the closed-loop system is 110 Hz. So, Eq. (16) is given by

$$K(S) = \frac{15(s + 1.36 \times 10^4)(s + 7.42 \times 10^4)}{(s + 9 \times 10^4)(s + 2.5 \times 10^4)}. \quad (19)$$

Figure 7 shows the Bode diagram of the open-loop and closed-loop systems. The bandwidth of the closed-loop system is improved to 110 Hz from 5 Hz of the open-loop system at the resonant frequency. The 2% settling time of the closed-loop system is decreased to 0.02 sec from 0.246 sec of the open-loop system. Also, the displacement of the sensing-comb electrodes of the closed-loop system is decreased as shown in Figure 8.

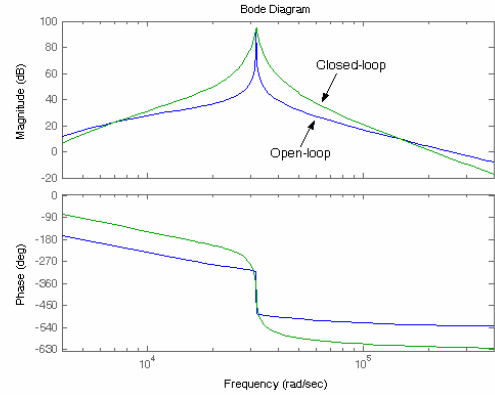


Fig. 7. Bode diagram of open-loop and closed-loop.

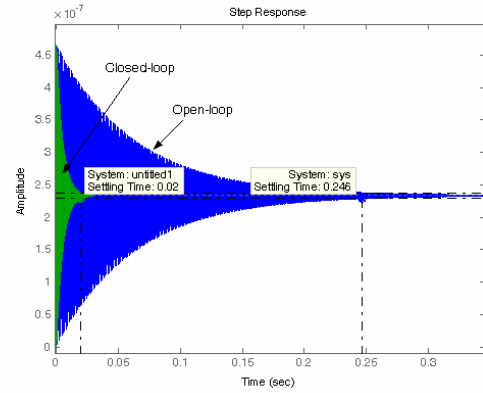


Fig. 8. Step response for displacement of sensing-comb electrodes.

## 5. SIMULATION RESULTS

We use the Matlab simulink as the simulation program. Figure 9 shows the simulink block diagram of the closed-loop system. When the input angular rate is 10 deg/sec, 5 Hz, Figure 10 shows the frequency response of the modulated output signal. The noise equivalent angular rate resolution of the closed-loop system is improved from 0.0021 deg/sec to 0.0013 deg/sec, when compared to the open-loop system. At this time, the average output signal level and the noise floor of open-loop system are -21.8 dB

and  $-95.5$  dB, and the average output signal level and the noise floor of closed-loop system are  $-10.3$  dB and  $-88.3$  dB.

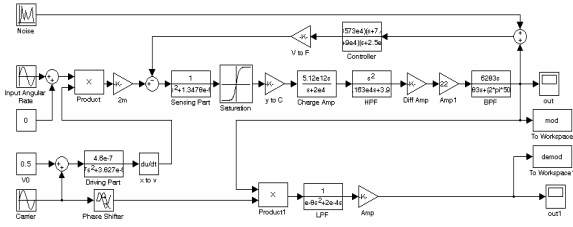
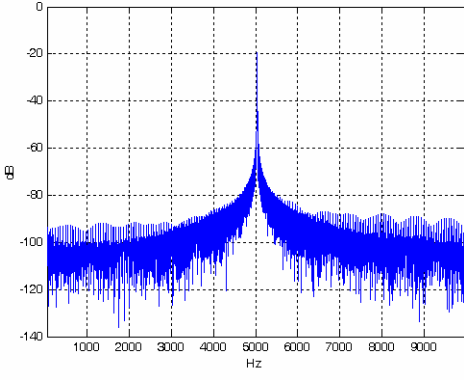
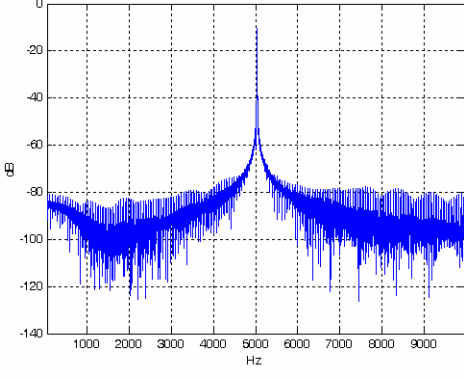


Fig. 9. Simulink block diagram of closed-loop.



(a) Open-loop system

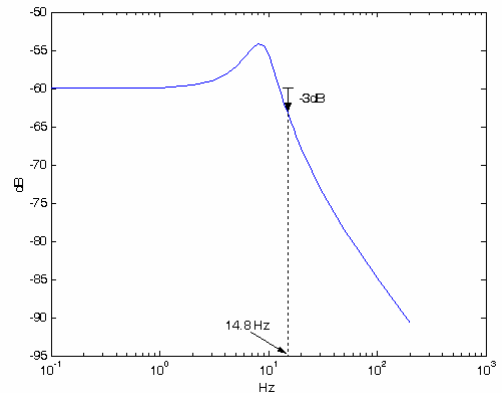


(b) Closed-loop system

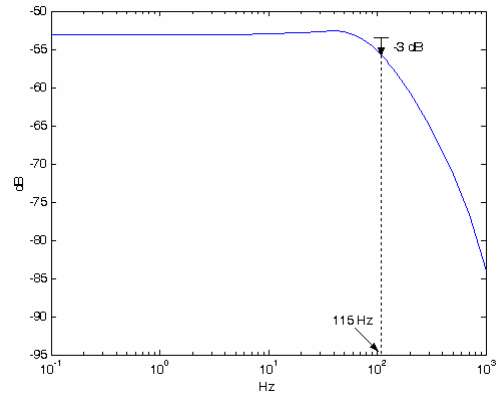
Fig. 10. Frequency response of modulated output signal.

Figure 11 shows the bode diagram of the demodulated output signal. This output signal is obtained by increasing the period of input angular rate. The bandwidth of the closed-loop system is improved from  $14.8$  Hz to  $115$  Hz. Figure 12 shows the demodulated output signal when the magnitude of input angular rate varies. The scale factor of the closed-loop system is increased to  $0.21$  mV/deg/sec from  $0.0986$  mV/deg/sec of the open-loop system. The input range is improved from  $\pm 50$  deg/sec to  $\pm 200$  deg/sec as shown in Figure 12, and thus, the dynamic range is improved from  $87.5$  dB to  $103.7$  dB. Also, the linearity of the closed-loop system is improved from  $7.25\%$  to  $0\%$  in the  $\pm 50$  deg/sec range. Finally, the bias stability tests are performed. The output signal without applied the input angular rate is obtained as shown in Figure 13. The bias

stability of the closed-loop system is improved from  $0.0249$  deg/sec to  $0.0028$  deg/sec.

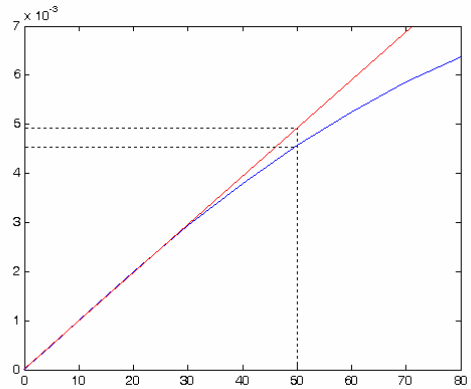


(a) Open-loop system

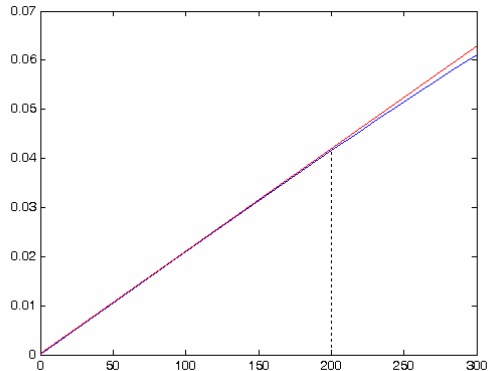


(b) Closed-loop system

Fig. 11. Bandwidth of output signal.



(a) Open-loop system



(b) Closed-loop system

Fig. 12. Linearity of output signal.

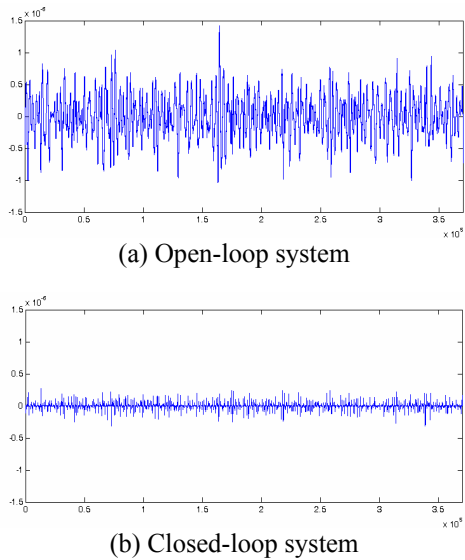


Fig. 13. Bias stability of output signal

## 6. CONCLUSION

This paper designed a lead-lag compensator for a MEMS microgyroscope. The design feedback controller greatly improves the bandwidth, linearity, dynamic range, and bias stability of the microgyroscope without sacrificing resolution, by feeding the control signal from the sensed output signal back to the sensing-comb electrodes. This controller can maintain the matched state of the driving and sensing modes, and therefore the expanded bandwidth can be achieved without lowering the sensitivity. As a result, the bandwidth of the closed-loop system is improved from 14.8 Hz to 115 Hz, the input range is improved from  $\pm 50$  deg/sec to  $\pm 200$  deg/sec, and the dynamic range is improved from 87.5 dB to 103.7 dB. The linearity is also improved from 7.25 % to 0 % in the  $\pm 50$  deg/sec range, and the bias stability is improved from 0.0249 deg/sec to 0.0028 deg/sec. These performance improvements are achieved without sacrificing the resolution, which also improves from 0.0021 deg/sec to 0.0013 deg/sec.

## ACKNOWLEDGMENTS

This research was supported in part by KOSEF Development of Telematics-based Integrated Sensing and Monitoring Systems Project (R01-2003-000-10109-0).

## REFERENCES

- Cho, Y. H., B. M. Kwak, A. P. Pisano, and R. T. Howe (1993). Viscous energy dissipation in laterally oscillating planar microstructures: A theoretical and experimental study. *Proc. IEEE Workshop on Microelectro-mech. Sys.*, pp. 93-99.
- Song, Cimoo. (1997). Commercial Vision of Silicon Based Inertial Sensors. *Proceedings of Transducers '97*, vol. 2, pp. 839 -842.
- Lee, S., S. Park, and D. Cho (1999). The Surface/Bulk Micromachining (SBM) process: a new method for fabricating released microelectromechanical systems in single crystal silicon. *IEEE/ASME Journal of Microelectromechanical Systems*, vol. 8, no. 4, pp. 409-416.
- Lee, S., S. Park, J. Kim, S. Yi, and D. Cho (2000). Surface/Bulk Micromachined Single-crystalline Silicon Micro-gyroscope. *IEEE/ASME Journal of Microelectromechanical Systems*, vol. 9, no. 4, pp. 557-567.
- Cho, D., S. Lee, and S. Park (2000). Surface/Bulk Micromachined High Performance Silicon Micro-gyroscope. *2000 Solid-state Sensor and Actuator Workshop (Hilton Head)*.
- Park, S., S. W. Lee, J. Kim, S. Lee, and D. Cho (2001). Tactical Grade MEMS Gyroscope Fabricated by the SBM Process. *International MEMS Workshop 2001*, pp. 168-177.
- Gripton, A. (2002). The Application and Future Development of A MEMS SiVSG for Commercial and Military Inertial Products. *Position Location and Navigation Symposium, 2002 IEEE*, pp. 28 -35.